



# 1 **A parameterization of sulfuric acid-dimethylamine nucleation** 2 **and its application in three-dimensional modeling**

3 Yuyang Li<sup>1, #</sup>, Jiewen Shen<sup>1, 2, #</sup>, Bin Zhao<sup>1, 2, \*</sup>, Runlong Cai<sup>3</sup>, Shuxiao Wang<sup>1, 2</sup>, Yang Gao<sup>4</sup>, Manish Shrivastava<sup>5</sup>, Da Gao<sup>1, 2</sup>,  
4 Jun Zheng<sup>6</sup>, Markku Kulmala<sup>2, 7, 8</sup>, Jingkun Jiang<sup>1, \*</sup>

5  
6 <sup>1</sup>State Key Joint Laboratory of Environment Simulation and Pollution Control, School of Environment, Tsinghua University,  
7 100084 Beijing, China

8 <sup>2</sup>State Environmental Protection Key Laboratory of Sources and Control of Air Pollution Complex, Beijing, 100084, China

9 <sup>3</sup>Institute for Atmospheric and Earth System Research/Physics, Faculty of Science, University of Helsinki, 00014 Helsinki,  
10 Finland

11 <sup>4</sup>Key Laboratory of Marine Environment and Ecology, Ministry of Education, Ocean University of China, Qingdao 266100,  
12 China

13 <sup>5</sup>Brian Gaudet, Pacific Northwest National Laboratory, Richland, Washington, USA

14 <sup>6</sup>School of Environmental Science and Engineering, Nanjing University of Information Science & Technology, Nanjing  
15 210044, China

16 <sup>7</sup>Aerosol and Haze Laboratory, Beijing Advanced Innovation Center for Soft Matter Science and Engineering, Beijing  
17 University of Chemical Technology, 100029 Beijing, China

18 <sup>8</sup>Joint International Research Laboratory of Atmospheric and Earth System Sciences, School of Atmospheric Sciences,  
19 Nanjing University, Nanjing, China

20 # These authors contributed equally

21 \* Correspondence to: Bin Zhao (bzha@mail.tsinghua.edu.cn) and Jingkun Jiang (jiangjk@tsinghua.edu.cn)



22 **Abstract.** Sulfuric acid (SA) is a governing gaseous precursor for atmospheric new particle formation (NPF) in diverse  
23 environments, which is a major source of global ultrafine particles. In polluted urban atmosphere with high condensation sink  
24 (CS), the formation of stable SA-amine clusters, such as SA-DMA clusters, usually initializes intense NPF events. Coagulation  
25 scavenging and cluster evaporation are dominant sink processes of SA-amine clusters in urban atmosphere, yet they are not  
26 quantitatively included in the present parameterizations of SA-amine nucleation. We herein report a parameterization of SA-  
27 DMA nucleation based on cluster dynamic simulations and quantum chemistry calculations, with certain simplifications to  
28 largely reduce the computational costs. Compared with previous SA-DMA nucleation parameterizations, this new  
29 parameterization would be able to reproduce the dependences of particle formation rates on temperature and CS. We then  
30 incorporated it in a three-dimensional chemical transport model to simulate the evolution of particle number size distributions.  
31 Simulation results show good consistency with the observations in the occurrence of NPF events and particle number size  
32 distributions in wintertime Beijing, showing a significant improvement compared to that using parameterization without  
33 coagulation scavenging. Quantitative analysis shows that SA-DMA nucleation contributes majorly to nucleation rates and  
34 aerosol population during the 3-D simulations in Beijing (>99% and >60%, respectively). These results broaden the  
35 understanding of NPF in urban atmospheres and stress the necessity of including the effects of coagulation scavenging and  
36 cluster stability in simulating SA-DMA nucleation in three-dimensional simulations. This would improve the performance in  
37 particle source apportionment and quantification of aerosol effects on air quality, human health, and climate.



## 38 **1 Introduction**

39 New particle formation (NPF) is the major source of atmospheric particles in terms of their number concentration, which  
40 regulates the Earth's radiative balance and affects the climate (Kulmala et al., 2004; Gordon et al., 2017; Merikanto et al.,  
41 2009). The transformation from gaseous precursors to stable clusters and particles via nucleation is the initial step of NPF, and  
42 new particle formation rate ( $J$ ) is an essential parameter to characterize NPF intensity (Kulmala, 2003). Although nucleation  
43 processes would be suppressed by coagulation scavenging in urban atmospheres with high condensation sink (CS) (Cai and  
44 Jiang, 2017; Cai et al., 2017b), intense NPF events have been frequently observed (Wu et al., 2007; Xiao et al., 2015; Deng et  
45 al., 2020). Recently, increasing evidence has been provided that those intense events are driven by the formation of stable SA-  
46 amine clusters (Cai et al., 2022; Jen et al., 2014b) with a speed close to the collision limit for SA molecules, thus deriving high  
47 nucleation rates in urban atmospheres (Cai et al., 2021d; Yao et al., 2018; Chen et al., 2012). Thus, integrating SA-amine  
48 nucleation into three-dimensional (3-D) models would be essential in extending the understanding of NPF in polluted urban  
49 areas and quantifying its underlying impacts on the environment and climate. This requires a quantitative representation of  
50 particle formation rates through SA-amine nucleation for 3-D models.

51 Semi-empirical power-law functions are widely used in SA-relevant nucleation rate studies to fit the experimental data, which  
52 has been shown to reproduce the measured  $J$  in certain ambient observations or experimental conditions (Riccobono et al.,  
53 2014; Dunne et al., 2016; Bergman et al., 2015; Hanson et al., 2017; Semeniuk and Dastoor, 2018; Kurten et al., 2014; Kurten  
54 et al., 2018). For SA-amine nucleation, Bergman et al. (2015) and Dunne et al. (2016) have presented semi-empirical  
55 parameterizations of good consistencies with chamber and flow-tube experimental results (Almeida et al., 2013; Jen et al.,  
56 2014b; Glasoe et al., 2015). In real urban atmosphere, recent advances have shown that coagulation scavenging would largely  
57 suppress concentrations of molecular clusters, and thus the nucleation rates (Cai and Jiang, 2017; Cai et al., 2021c; Cai et al.,  
58 2021d; Marten et al., 2022). It has also been addressed that the formation of the smallest SA-amine clusters, which is largely  
59 dependent on cluster stability, is the limiting step for SA-amine nucleation rates (Cai et al., 2022). However, the effects of  
60 coagulation scavenging and cluster stability would vary with the environmental factors, e.g., CS and temperature, while these  
61 effects have not been well represented in semi-empirical power-law functions derived from certain experimental systems or  
62 ambient environments. Cluster kinetic simulations coupled with quantum chemistry calculations (Mcgrath et al., 2012), which  
63 take into account the effects of both coagulation scavenging and cluster stability, have been widely applied in zero-dimensional  
64 or one-dimensional simulations of SA-NH<sub>3</sub> or SA-amine nucleation (Yang et al., 2021; Lu et al., 2020; Yao et al., 2018; Yu,  
65 2006; Yu and Turco, 2001). Specifically, both cluster kinetic simulations and observations reveal that dimethylamine (DMA)  
66 is plausibly most efficient in stabilizing SA clusters and is regarded as the key amine species deriving high particle formation  
67 rates in urban atmosphere (Jen et al., 2014b; Cai et al., 2022; Yao et al., 2018; Chen et al., 2012). However, no method with  
68 good representations of coagulation scavenging and cluster stabilities has been reported to explicitly simulate the SA-DMA  
69 nucleation rates in 3-D chemical transport models.

70 A challenge in setting up a parameterization based on cluster kinetic simulations for 3-D chemical transport models is to reduce  
71 computational costs and yield explicit expressions. A plausible method to reduce computational costs is to omit the unstable  
72 clusters with high evaporation rates from the nucleation pathway. Accordingly, different nucleation schemes were presented  
73 to represent the dominant source or sink processes of SA-DMA clusters in specific chamber experiments or ambient  
74 environments (Lu et al., 2020; Cai et al., 2021d). For polluted urban atmospheres, a kinetic model with a key pathway of  
75 particle formation in SA-DMA nucleation was constructed, yielding good predictions of measured SA cluster concentrations  
76 and 1.4 nm particle formation rates ( $J_{1.4}$ ) in urban Beijing (Cai et al., 2021d). Application of pseudo-steady-state assumptions  
77 is also an alternative method for reducing computational costs and yielding explicit expressions. The NPF occurrence indicator  
78 ( $I$ ) based on the kinetic model with pseudo-steady-state assumptions has shown good consistency in qualitatively estimating  
79 the NPF events in urban Beijing and Shanghai (Cai et al., 2021c). These results indicate the potential of deriving an explicit



80 parameterization of particle formation rates by applying pseudo-steady-state assumptions to the kinetic model, although further  
81 quantitative analysis is still required to validate this parameterization.

82 In this study, we set up an SA-DMA nucleation parameterization, which is designed for application in 3-D chemical transport  
83 models. The parameterization is based on the pseudo-steady-state particle formation rate in the kinetic model, with a full  
84 representative of the effects of coagulation scavenging and cluster stability (Cai et al., 2021d). Generally, only four variables  
85 (temperature  $T$ , CS, gaseous DMA concentrations  $[B]$ , and concentrations of SA molecules or clusters containing one SA  
86 molecule  $[SA_{tot}]$ ) are used in the parameterization, with computational costs largely reduced. We then implement the  
87 parameterization in a 3-D chemical transport model and combine it with an integrated source-sink representation of DMA to  
88 simulate the evolution of the particle number size distributions (PNSDs) in wintertime Beijing. The precursor concentrations,  
89 PNSDs, NPF occurrence and  $J_{1,4}$  show relatively good consistencies between simulations and observations. The simulations  
90 show that the SA-DMA nucleation contributes >99% of the  $J_{1,4}$  and >60% of the total particle number concentration in  
91 wintertime Beijing, respectively. With this parameterization, 3-D chemical transport models could significantly improve the  
92 simulation of NPF, especially in urban environments, and thus the effects of NPF on particulate matter pollution or climate.

## 93 2 Methods

### 94 2.1 Derivation of Parameterized Formation Rate in SA-DMA Nucleation

95 Limited by computational quantum chemistry calculation results, SA-DMA nucleation is commonly simulated in the range of  
96 clusters containing not more than 4 SA or 4 DMA molecules (Olenius et al., 2013; Ortega et al., 2012). As unstable clusters  
97 would evaporate with higher rates, the formation of larger clusters potentially follows the pathways of the most stable clusters.  
98 In addition, as the SA-DMA clusters are increasingly stable along the main pathway of cluster formation, the clusters not  
99 smaller than  $A_4B_4$  (hereafter  $A_mB_n$  refers to clusters containing  $m$  SA and  $n$  DMA molecules) is assumed to not evaporate back  
100 in these simulations. Although there are uncertainties in the pathways presented based on different quantum chemistry methods,  
101 it is well accepted that the  $A_mB_m$  ( $m=1$  to 4) and  $A_2B_1$  clusters are relatively stable in the SA-DMA nucleation scheme (Olenius  
102 et al., 2017; Olenius et al., 2013; Ortega et al., 2012; Myllys et al., 2019).

103 Accordingly, the parameterization in this study is derived from the nucleation pathway including  $A$ ,  $B$  and other 5 SA-DMA  
104 clusters ( $A_mB_m$  ( $m=1$  to 4) and  $A_2B_1$ ), consistent with a previous study (Cai et al., 2021d). The clusters except  $A_4B_4$  are assumed  
105 to be in pseudo-steady-states, i.e. the sink due to evaporation, coagulation scavenging, and cluster collision is equal to the  
106 source due to the collisions of molecules or smaller clusters. As the  $A_4B_4$  clusters are estimated to be with an electrical mobility  
107 diameter of approximately 1.4 nm, the pseudo-steady-state formation rate of  $A_4B_4$  would be applied in the parameterization of  
108  $J_{1,4}$  in this study.

#### 109 2.1.1 Derivation of Collision Coefficients, Coagulation Sink, and Evaporation Rates

110 In the nucleation pathway discussed above,  $A$ ,  $B$ , and 5 SA-DMA clusters are included. The collision coefficients between  
111 them ( $\beta_{i-j}$ ) and the evaporation rate of  $A_1B_1$  clusters ( $\gamma$ ) would vary with  $T$  during the simulation. The coagulation sinks (Coag $S_i$ )  
112 due to the coagulation scavenging of background aerosols are dependent on CS. The work discussed in this section is focused  
113 on simplification of the derivation of these parameters to be updated in each simulation time interval to reduce the  
114 computational costs.

115 As the involved clusters and molecules are in the free molecular regime (Knudsen number > 10),  $\beta_{i-j}$  in SA-DMA nucleation  
116 processes can be calculated based on kinetic gas theory (Seinfeld and Pandis, 1998; Olenius et al., 2013; Ortega et al., 2012):



$$117 \quad \beta_{i,j} = \left(\frac{3}{4\pi}\right)^{1/6} \left(\frac{1}{m_i} + \frac{1}{m_j}\right)^{1/2} (V_i^{1/3} + V_j^{1/3})^2 (6k_b T)^{1/2} E_{ij}, \quad (1)$$

118 where  $m$  (kg) and  $V$  (m<sup>3</sup>) represent the molecular mass and molecular volume, respectively. The density of precursor molecules  
119  $A$  and  $B$  was assumed to be 1830 and 680 kg m<sup>-3</sup>, respectively.  $T$  (K) represents the temperature.  $k_b$  (J K<sup>-1</sup>) is the Boltzmann  
120 constant. Subscripts  $i$  and  $j$  refer to the index of the clusters or molecules (1 to 7 refer to  $A$ ,  $B$ ,  $A_1B_1$ ,  $A_2B_1$ ,  $A_2B_2$ ,  $A_3B_3$ , and  $A_4B_4$ ,  
121 respectively, which are involved in the kinetic model).  $E_{ij}$  is a dimensionless enhancement factor of the collision rates from  
122 Van de Waals forces between  $i$  and  $j$ . In this study,  $E_{ij}$  is assumed to be 2.3 (Chan and Mozurkewich, 2001; Sceats, 1989),  
123 within the range of 2.3 to 2.7 predicted by Brownian coagulation models, and consistent with the value used in other cluster  
124 dynamics studies (Kurten et al., 2014; Lehtipalo et al., 2016; Stolzenburg et al., 2020).

125 Noting that  $m_i$  and  $V_i$  are almost independent of the atmospheric conditions and  $E_{ij}$  is assumed to be constant, we can normalize  
126 different values of  $\beta_{i,j}$  into  $\beta$ , and the normalizing factor is shown in a look-up table (Table S1 in the supporting information  
127 (SI)) as  $G(i,j)$ :

$$128 \quad \beta_{i,j} = \beta G(i,j), \quad (2)$$

129 where  $\beta$  represents the collision coefficients between two  $A_1B_1$  clusters ( $\beta_{3,3}$ ), and could be calculated as:

$$130 \quad \beta = \beta_0 \left(\frac{T}{T_0}\right)^{0.5}, \quad (3)$$

131 where  $\beta_0$  is the value of  $\beta$  at the standard temperature  $T_0=298.15$  K, constant as  $1.126 \times 10^{-15}$  m<sup>3</sup> s<sup>-1</sup>.

132 Similarly, CoagS<sub>*i*</sub> could also be normalized to CS using fixed ratios. The size dependent coagulation sink (CoagS) is calculated  
133 with a power-law exponent of -1.7, within the typical range of atmospheric aerosols (Lehtinen et al., 2007):

$$134 \quad \text{CoagS}_i = \text{CS} \left(\frac{V_i}{V_1}\right)^{1.7} = H(i) \text{CS}, \quad (4)$$

135 where the dimensionless factors  $H(i)$  are also recorded in Table S1 in the SI.

136 The evaporation rates of  $A_1B_1$  could be derived based on collision-evaporation equilibrium (Ortega et al., 2012), closely  
137 relevant to the free energy barrier to form  $A_1B_1$  clusters (Olenius et al., 2013; Ortega et al., 2012):

$$138 \quad \gamma = \beta_{1,2} c_{\text{ref}} \exp\left(\frac{\Delta G}{k_B T}\right), \quad (5)$$

139 where  $c_{\text{ref}}$  is the number concentrations under standard conditions ( $2.46 \times 10^{25}$  m<sup>-3</sup>).  $\Delta G$  is the formation free energies of  $A_1B_1$ .  
140 Thus if we take  $T_0 = 298.15$  as a reference,  $\gamma$  could also be calculated as:

$$141 \quad \gamma = \gamma_0 \left(\frac{T}{T_0}\right)^{0.5} \exp\left(\frac{\Delta H}{k_B} \left(\frac{1}{T} - \frac{1}{T_0}\right)\right), \quad (6)$$

$$142 \quad \gamma_0 = \gamma'_0 \exp\left(\frac{\Delta G - \Delta G_0}{k_B T_0}\right), \quad (7)$$

143 where  $\gamma'_0$ , with the value of  $3.33$  s<sup>-1</sup>, is the evaporation rates of  $A_1B_1$  at  $T_0$  with  $\Delta G = \Delta G_0 = -13.54$  kcal mol<sup>-1</sup>.  $\Delta H$  is the formation  
144 enthalpies of  $A_1B_1$ . In previous studies, several sets of  $\Delta H$  and  $\Delta G$  at specific temperatures were reported based on different  
145 quantum chemistry models. Here we use  $\Delta H = -24.82$  kcal mol<sup>-1</sup> and  $\Delta G = -13.54$  kcal mol<sup>-1</sup> according to the results in Myllys  
146 et al. (2019). If the values of  $\Delta G$  need to be updated in future application of this parameterization, the values of  $\gamma_0$  should be  
147 updated as well based on Eq. 7. The sensitivity analysis of different values of  $\Delta H$  and  $\Delta G$  are discussed in the Results section.

148 Generally, with  $G(i,j)$  and  $H(i)$  fixed into the parameterization formula,  $\beta_{i,j}$  and CoagS<sub>*i*</sub> could be normalized to  $\beta$  and CS.  
149 Additionally, the values of  $\gamma$  and  $\beta$  could be real-time updated at any simulation timestep based on Eqs. 3 and 6.

### 150 2.1.2 Formula of the SA-DMA Nucleation Parameterization

151 Applying the pseudo-steady-state assumptions to the key pathway discussed above (Eqs. S1 to S9) and achieving real-time  $\gamma$   
152 (s<sup>-1</sup>) and  $\beta$  (m<sup>3</sup> s<sup>-1</sup>) (Eqs. 3 and 6), we could derive an explicit formula of the parameterized  $J_{1,4}$  in this study (Eq. 8).



$$153 \quad J_{1.4} = \frac{\beta\theta[A_1B_1]^4}{2([A_1B_1]+0.39\frac{CS}{\beta})} \left( \frac{0.23\theta}{[A_1B_1]+0.39\frac{CS}{\beta}} + \frac{1.00}{[A_1B_1]+0.31\frac{CS}{\beta}} \right), \quad (8)$$

154 The above intermediate parameters are calculated as below:

$$155 \quad [A_1B_1] = \frac{0.96[B][SA_{tot}]}{0.96[B]+\frac{2}{\beta}+0.86[SA_{tot}]+0.63\frac{CS}{\beta}}, \quad (9)$$

$$156 \quad \theta = 1 + \frac{2[B]}{1.16[B]+0.46\frac{CS}{\beta}} \frac{[SA_{tot}]-[A_1B_1]}{[A_1B_1]}, \quad (10)$$

$$157 \quad \theta' = \frac{\theta(2.22[A_1B_1]+0.86\frac{CS}{\beta})}{\sqrt{(1.11[A_1B_1]+0.43\frac{CS}{\beta})^2+1.12\theta[A_1B_1]^2+1.11[A_1B_1]+0.43\frac{CS}{\beta}}}, \quad (11)$$

158 In Eqs. 8 to 11, the four input variables ( $T$  (K),  $CS$  ( $s^{-1}$ ),  $[B]$  ( $m^{-3}$ ),  $[SA_{tot}]$  ( $m^{-3}$ )) are shown in bold. Generally, only these four  
159 variable parameters are needed for the 3-D chemical transport models. Additionally, compared with directly coupling cluster  
160 dynamic simulations into 3-D chemical transport models, the parameterization of pseudo-steady-state  $J_{1.4}$  requires much less  
161 computational time.

## 162 2.2 Incorporating the Parameterization into Updated WRF-Chem/R2D-VBS Model

163 The updated parameterization of SA-DMA nucleation was incorporated in the WRF-Chem (Weather Research and Forecasting  
164 model with Chemistry). Before adding the SA-DMA nucleation, we already incorporated seven other NPF mechanisms in the  
165 model (Zhao et al., 2020): four inorganic pathways, including binary neutral/ion-induced SA-H<sub>2</sub>O nucleation and ternary  
166 neutral/ion-induced NH<sub>3</sub>-SA-H<sub>2</sub>O nucleation; and three organic pathways, including pure-organic neutral/ion-induced organic  
167 nucleation and ternary nucleation involving organics and SA. The organic containing nucleation pathways are driven by ultra-  
168 and extremely low volatility organic compounds (ULVOC and ELVOC) with O:C > 0.4, converted from monoterpene  
169 autoxidation. The chemical transformation and volatility distribution of monoterpene is represented in the model by R2D-VBS  
170 (Radical Two-Dimensional Volatility Basis Set framework) with constrained parameters against experiments. More details of  
171 the R2D-VBS are given in our previous study (Zhao et al., 2020). The newly formed nano-sized particles and their initial size  
172 evolution are accounted in the MOSAIC module by 20 size bins covering 1 nm to 10  $\mu$ m. It is worth mentioning that the newly  
173 formed particles from SA-DMA nucleation are lumped into a lower aerosol size bin in the model than that of other seven  
174 pathways. This should be attributed to that our SA-DMA nucleation parameterization are formulated at a 1.4 nm-sized particle  
175 formation rate while the remaining ones are fitted based on measured particle formation rates from CLOUD Chamber at a  
176 mobility diameter of 1.7 nm. Given that condensation of gaseous SA and DMA on pre-existing aerosols and nucleation occur  
177 simultaneously in real atmosphere, in the model, we then use a time-integrated-averaged concentration of precursors over each  
178 time step to drive SA-DMA nucleation. The condensation sink for SA and DMA is calculated according to simulated real-  
179 time PNSDs. In addition, the consumption of both SA and DMA concentration during nucleation is also accounted in the  
180 model, in order to represent a comprehensive sources-sink simulation scheme of two precursors in combination with other  
181 settings.

### 182 2.2.1 Sources and Sinks of Dimethylamine in the Updated WRF-Chem/R2D-VBS Model

183 A regional or global bottom-up emission inventory of DMA is currently lacking, mostly due to scarce direct measurements  
184 (Yang et al., 2022; Zhu et al., 2022). In previous 3D model studies, amine/NH<sub>3</sub> emission ratios have often been used to estimate  
185 amine emissions due to the close correlation between NH<sub>3</sub> and DMA emissions. However, a fixed amine/NH<sub>3</sub> ratio is likely  
186 to overestimate the concentrations of amines in rural areas while underestimating those in urban areas, where high  
187 concentrations of amines have been reported (Yao et al., 2018; Bergman et al., 2015). Here, a set of source-dependent



188 DMA/NH<sub>3</sub> emission ratio was used to develop the emission inventory of DMA based on (Mao et al., 2018). The ratios for  
189 different emission sectors were determined by a source apportionment analysis, based on a simultaneous observation of NH<sub>3</sub>,  
190 C1-C3 amines, NO<sub>x</sub>, and SO<sub>2</sub> and also meteorological factors at a suburban site in Nanjing (Zheng et al., 2015a). We applied  
191 the source-dependent emission ratios (0.0070, 0.0018, 0.0015, 0.0100, and 0.0009 for chemical–industrial, other industrial,  
192 agricultural, residential, and transportation source types, respectively) to NH<sub>3</sub> emissions in the ABaCAS-EI 2017 (Emission  
193 Inventory of Air Benefit and Cost and Attainment Assessment System) for China mainland and the IASA 2015 emission  
194 inventory for other areas to build continental DMA emission inventory (Zheng et al., 2019; Gao et al., 2020). In addition,  
195 DMA emission for maritime area was developed employing a DMA/NH<sub>3</sub> ratio derived from recent campaigns in offshore  
196 areas of China (see details in SI) (Chen et al., 2021).

197 DMA can be removed from the atmosphere through three main pathways: gas-phase chemical reaction, aerosol uptake, and  
198 wet deposition, which are all explicitly considered in our model. For the gas-phase chemical reactions, only oxidation of DMA  
199 by •OH is included. Reactions with other oxidants (O<sub>3</sub> and NO<sub>3</sub>) are much slower and therefore have negligible effects on  
200 DMA concentrations (Ge et al., 2011). The mechanism of DMA concentration depletion by aerosol uptake is still poorly  
201 understood, and the key parameter, uptake coefficient  $\gamma_u$ , varies in a wide range depending on many factors such as aerosol  
202 composition and relative humidity. In this study, we assumed  $\gamma_u = 0.001$ , approximately a median value among those reported  
203 by recent laboratory measurements (Qiu et al., 2011; Wang et al., 2010). Regarding DMA depletion by wet deposition, the  
204 treatment is similar to that of NH<sub>3</sub> based on Henry's Law. The key parameters for above sink processes are summarized in  
205 Table S2 in the SI.

### 206 2.2.2 Configuration of the Updated WRF-Chem/R2D-VBS Model.

207 The WRF-Chem model configured with the SA-DMA nucleation is applied to a domain covering eastern Asia with a horizontal  
208 resolution of 27 km, where Beijing is located close to the center. The simulations are performed for two winter months  
209 separately (December 2018 and January 2019) with 5 days spin-up run for each month. The ABaCAS-EI 2017 and IASA  
210 2015 emission inventory were used for China mainland and other areas, respectively. The biogenic emission is calculated by  
211 the Model of Emissions of Gases and Aerosols from Nature (MEGAN) v2.04 (Guenther et al., 2006). Except for the  
212 monoterpene-related gas and aerosol chemistry that is traced by R2D-VBS, the remaining gas- and aerosol chemical processes  
213 are simulated by the SAPRC99 gas chemistry scheme coupled with the MOSAIC (Model for Simulating Aerosol Interaction  
214 and Chemistry) aerosol module and a one-dimensional VBS set for SOA modeling (Zaveri et al., 2014; Shrivastava et al.,  
215 2019; Shrivastava et al., 2011).

216 Four scenario simulations with different configurations of the NPF mechanisms were conducted in this study to examine how  
217 the SA-DMA nucleation affects the simulations of aerosol size distribution: 1) 8 NPF mechanisms with the SA-DMA  
218 nucleation rate at 1.4 nm (abbr. DMA1.4\_Mech8); 2) 8 NPF mechanisms with the SA-DMA nucleation rate at 1.7 nm  
219 converted using modified Kerminen-Kulmala equation (Lehtinen et al., 2007) (DMA1.7\_Mech8); 3) 7 NPF mechanisms  
220 without the SA-DMA nucleation (NoDMA\_Mech7); and 4) No NPF mechanism (NoDMA\_Mech0). Among them, scenario 1  
221 is our “best-case” with a full consideration of available nucleation mechanisms; scenario 2 is set to probe the feasibility to use  
222 modified Kerminen-Kulmala equation to simulate the initial particle growth; scenario 3 is the “base-case” representing the  
223 performance of the original model; and scenario 4 represents the evolution of aerosol population only contributed by primary  
224 emission. Scenarios 3 and 4 were set as controlling groups to assess the role of SA-DMA nucleation and other mechanisms.

### 225 2.3 Ambient Measurements

226 Ambient observations were conducted at an urban site in Beijing from January 2018 to April 2018 and from October 2018 to  
227 March 2019. The site is located on the West Campus of Beijing University of Chemical Technology. Details of the observation  
228 site can be found in previous studies (Liu et al., 2020; Deng et al., 2020). The concentrations of SA and involving clusters are



229 measured using a chemical ionization high resolution time of flight mass spectrometer (CI-HTOF-MS) and a chemical  
230 ionization time of flight mass spectrometer with a long mass analyzer (CI-LTOF-MS) (Bertram et al., 2011; Jokinen et al.,  
231 2012). Other details in the sampling configurations have been reported in our previous study (Deng et al., 2020). Amine  
232 concentrations are measured using a modified time of flight mass spectrometer (TOF-MS) (Zheng et al., 2015b; Cai et al.,  
233 2021b). A weather station was deployed to measure the meteorological data, including ambient temperature, relative humidity  
234 and pressure. The PNSDs of particles from 1 nm to 10  $\mu\text{m}$  were measured using a particle size distribution (PSD) and a diethyl  
235 glycol-scanning mobility particle sizer (DEG-SMPS) (Jiang et al., 2011; Liu et al., 2016; Cai et al., 2017a). CS is calculated  
236 from the measured PNSDs and  $J_{1,4}$  is calculated using an improved aerosol population balance formula (Cai and Jiang, 2017).  
237 The details of instrument calibrations and data validations can be found in our previous study (Cai et al., 2021b).

### 238 3 Results and discussion

#### 239 3.1 Validation of Parameterization

240 The reasonability of pseudo-steady-state assumptions in the SA-DMA nucleation pathway was tested through comparisons  
241 between the characteristic equilibrium time ( $\tau$ ) of kinetic simulation (see details in the *SI*) and the data collection time interval.  
242 The characteristic equilibrium time of involving clusters and simulated  $J_{1,4}$  were shown in Fig. S1 in the *SI*. Generally, in either  
243 clean and cold circumstances or polluted and warm circumstances, the kinetically simulated  $J_{1,4}$  could be well reproduced by  
244 parameterized pseudo-steady-state  $J_{1,4}$ . Actually,  $\tau$  would vary greatly with CoagS and  $\gamma$ , and would be higher on cleaner and  
245 colder days, while even in extremely clean and cold days with  $CS = 0.0001 \text{ s}^{-1}$  and  $T = 255 \text{ K}$ ,  $\tau$  of  $A_3B_3$  (longer than other  
246 clusters) is only  $\sim 20$  min, shorter than the data collection time interval of 30 min. Thus for circumstances where there are high  
247 atmospheric concentrations of DMA and SA, such as most typical polluted regions, we conclude that nucleation processes are  
248 rapid enough that kinetic  $J_{1,4}$  can be represented by pseudo-steady-state  $J_{1,4}$ .

249 Figure 1 presents the comparisons between parameterized  $J_{1,4}$  in this study and those simulated in the kinetic models (hereafter  
250 referred to as KM) presented by Cai et al. (2021) and the cluster dynamic simulations containing all  $A_mB_n$  ( $m, n \leq 4$ ) clusters  
251 (hereafter referred to as CDS). The simulated  $J_{1,4}$  in KM can be reproduced by parameterized  $J_{1,4}$  within a  $\pm 50\%$  range for  
252 most of the cases in urban Beijing, with no systematic deviations found between them.

253 Figure 1b shows that for most of the circumstances, deviations between the parameterized  $J_{1,4}$  and  $J_{1,4}$  simulated in CDS are  
254 within a range of 1 order of magnitude. However, for circumstances with high temperatures, the parameterized  $J_{1,4}$  would be  
255 higher than those simulated in CDS, which might be due to that the  $A_kB_k$  ( $k=2,3$  and 4) clusters are assumed to be non-  
256 evaporative in KM while they would evaporate back in CDS under high temperatures. The reasonability of cluster stability  
257 assumptions under high temperatures relies mainly on the accuracy of quantum chemistry calculations, which requires more  
258 experimental evidence and discussions. Additionally, due to the negative dependence of simulated  $J_{1,4}$  on  $T$ , the simulated  $J_{1,4}$   
259 in this parameterization would be mostly lower than  $10 \text{ cm}^{-3}\text{s}^{-1}$  under temperatures higher than  $15 \text{ }^\circ\text{C}$ , lower than the median  
260 and mean value of particle formation rates measured during long-term observations in Beijing (Deng et al., 2021). Although  
261 they are relatively higher than those simulated in CDS, the simulation results of NPF occurrence would not show large  
262 deviations.

263 The computational costs of these three simulations have also been tested on the same personal computer with a Matlab program.  
264 To achieve the steady-state  $J_{1,4}$  in a specific atmospheric condition, the CDS and KM needs  $\sim 10$  s and  $\sim 0.05$  s CPU time,  
265 respectively, while the calculation of parameterized pseudo-steady-state  $J_{1,4}$  merely costs  $\sim 2 \times 10^{-7}$  s CPU time. The CPU time  
266 was reduced by a factor of  $5 \times 10^7$  and  $4 \times 10^4$  compared to CDS and KM, respectively. Thus introducing this parameterization  
267 into 3-D chemical transport models could largely reduce the computational costs.



### 268 3.2 The Dependence of Parameterized $J_{1,4}$ on Input Parameters

269 The correlation between parameterized SA-DMA nucleation  $J_{1,4}$  and the input parameters are shown in Fig. 2. The parameters  
270 involved are  $T$ , CS, [DMA], and [SA]<sub>tot</sub>. The mean values of measured data during the observation period (281K, 0.02 s<sup>-1</sup>, 3  
271 ppt, and 3.5×10<sup>6</sup> cm<sup>-3</sup>, respectively) are applied as typical conditions in the base case. Different from the semi-empirical power-  
272 law functions only based on precursor concentrations presented by Dunne et al. (2016), the dependences of particle formation  
273 rates on  $T$  and CS are represented in our parameterizations. With  $T$  increasing from -10 to 20 °C,  $\gamma$  would increase by ~2 orders  
274 of magnitude, as shown in Fig. 2a, and thus  $J_{1,4}$  would decrease by over 2 orders of magnitude. The decreasing trend of  
275 observed NPF rate ( $J_{1,5}$  in this case) as a function of increasing  $T$  in urban Beijing has also been reported (Deng et al., 2020),  
276 consistent with our parameterizations.

277 Fig. 2b shows that  $J_{1,4}$  would decrease by 2-4 orders of magnitude with CS increasing by a factor of 10, and the logarithm  
278 dependence is higher in circumstances with higher CS, such as urban Beijing, where CoagS dominates the sinks. This is  
279 consistent with the negative CS dependence of measured particle formation rates and NPF occurrence demonstrated in previous  
280 observations in Beijing (Deng et al., 2021; Cai et al., 2021b; Cai et al., 2021a).

281 The parameterized  $J_{1,4}$  shows an increasing trend with increasing concentrations of SA and DMA. Parameterized  $J_{1,4}$  is  
282 approximately proportional to [SA]<sup>4</sup>, while the dependence of  $J_{1,4}$  on [DMA] is decreasing with increasing [DMA]. This is  
283 due to the near-saturation formation of A<sub>1</sub>B<sub>1</sub> clusters, which is also found in kinetic model simulation results (Cai et al., 2021d).  
284 Generally, the parameterization could reproduce the fact that SA-DMA nucleation is driven by SA-DMA cluster formation,  
285 dominantly suppressed by cluster evaporation and coagulation sinks.

### 286 3.3 Comparison of 3D Model Simulations with Observations

287 As DMA and SA concentrations are key input variables for the SA-DMA nucleation parameterization, we first compare  
288 simulated DMA and SA concentrations from the DMA1.4\_Mech8 scenario with observations (Fig. 3). Generally, there are  
289 good consistencies of both mean concentrations and temporal variations, although there are still deviations at certain times.  
290 The mean simulated concentrations of DMA and SA are 1.9 ppt and 1.4×10<sup>6</sup> cm<sup>-3</sup>, respectively, close to observed  
291 concentrations of 2.0 ppt and 1.6×10<sup>6</sup> cm<sup>-3</sup>. This proves the validity of the comprehensive representation of source-sink  
292 behaviors of DMA in the model.

293 The time series of PNSDs for different simulation scenarios are presented in Fig. 4. When SA-DMA nucleation is considered,  
294 the typical PNSDs shape in observed NPF days (12/07, 12/08, 12/09, 01/20, and 01/21), characterized as the burst of  
295 nanometer-sized particles and subsequent growth, are well captured by our “best-case” scenario DMA1.4\_Mech8 and also  
296 DMA1.7\_Mech8. By contrast, the scenarios without DMA-SA nucleation, NoDMA\_Mech7 and NoDMA\_Mech0, cannot  
297 reproduce the observed NPF events with a “vacancy band” for 1~10 nm size range over the entire simulation period. Actually,  
298 although there are slightly higher sub-3 nm particle concentrations in NoDMA\_Mech7 than those in NoDMA\_Mech0, which  
299 are generated from the 7 nucleation pathways other than DMA-SA nucleation, the newly formed particle concentrations are  
300 too low to survive in the subsequent growth and be separated from background aerosols in the PNSDs. These results  
301 demonstrate that SA-DMA nucleation should be the dominant mechanism during NPF events in Beijing compared with other  
302 7 mechanisms.

303 Our results also reproduce the dependence of NPF occurrence on CS in Beijing. As shown in Fig. S2 in the SI, NPF generally  
304 occurs at low CS while high CS results in too low nucleation rates to initiate NPF. Note that the simulated sub-3 nm particle  
305 concentrations also increase slightly on some non-NPF days in DMA1.4\_Mech8 and DMA1.7\_Mech8 scenarios, however,  
306 the concentrations are ~1 order of magnitude lower than those on NPF days and the newly formed particles also fail to survive  
307 in the subsequent growth. The improvements of using the nucleation parameterization in this study is further stressed in the



308 comparison between DMA1.4\_Mech8 scenario and the scenario (CLOUD) using the parameterization from Dunne et al.  
309 (2016). Figure S3 has shown that almost no rapid nucleation processes and NPF events are found in the simulation of CLOUD  
310 scenarios. In addition to the underestimation of nucleation rates, the simulated high nucleation rates usually occur on observed  
311 non-NPF days (Fig.S6), which should be attributed to the ignorance of CS dependence in the power-law function  
312 parameterizations.

313 Figure 5 further compares the simulated and observed PNSDs averaged over the simulation period. The “best-case” scenario  
314 DMA1.4\_Mech8 brings the averaged PNSD in 1~200 nm size range much closer to the observation than those of “base-case”  
315 NoDMA\_Mech7, and the latter only shows a minor change compared to scenario NoDMA\_Mech0 without any nucleation.  
316 One may notice that the averaged PNSD in 2~10 nm size range for scenario DMA1.4\_Mech8 is still lower than that of  
317 observation by ~1 order of magnitude, despite the good agreement in number concentrations of particles of ~1.4 nm. This  
318 could be attributed to two possible reasons: the model underestimates the actual nucleation rates; or newly formed particles of  
319 ~1.4 nm grow too fast to larger size bins in the model (> 10 nm). The first one can be excluded by a generally good agreement  
320 between simulated nucleation rates and ones derived from observation, even with a slightly higher mean value for the former  
321 (shown in next section, Fig. 6). Hence, the gap in 2~10 nm size range might be attributed to the particle growth simulations in  
322 the model which deserves further improvement. Moreover, in spite of similar performance in improving PNSDs simulations  
323 compared to the “best-case” DMA1.4\_Mech8, the scenario of DMA1.7\_Mech8 presents a shifted PNSD pattern to larger size  
324 range. For these two scenarios including SA-DMA nucleation, scenario DMA1.4\_Mech8 is more reasonable since a systematic  
325 underestimation exists over the entire 1~10 nm range in scenario DMA1.7\_Mech8. Still, the conversion from 1.4 nm rate to  
326 those for larger particles through modified Kerminen-Kulmala equation is an alternative way to depict SA-DMA nucleation  
327 for other models with different aerosol size settings. Overall, despite aforementioned deficiencies, our updated WRF-  
328 Chem/R2D-VBS model configured with the SA-DMA nucleation parameterization shows substantial improvement in  
329 representation of NPF events and the PNSD.

### 330 3.4 Contribution from Various Pathways to Nucleation Rates and Particle Number Concentrations

331 Quantitative analysis over various nucleation pathways is performed here to improve the understanding of NPF in Beijing. As  
332 presented in Fig. 6, the variation of nucleation rates, which are derived from observed PNSD data, is well represented by the  
333 best-case scenario DMA1.4\_Mech8. Compared to the vast majority contribution from SA-DMA nucleation, the nucleation  
334 rates from other nucleation mechanisms are lower by a factor of ~100. In addition, SA-DMA nucleation contributes over 60%  
335 to aerosol population, reinforcing its dominant role in modulating aerosol population in urban atmosphere.

### 336 3.5 Sensitivity Analysis

337 Having shown the significant improvement of model performance in simulating NPF by coupling the SA-DMA nucleation  
338 parameterization, we acknowledge that the simulation of SA-DMA nucleation in 3D model still has uncertainties in terms of  
339 both source-sink representation of DMA and nucleation parameterization. Here, several key factors which may alter model  
340 performance were selected to perform sensitivity analysis.

341 First, the uncertainties brought by  $\Delta G$  achieved from different quantum chemistry results are tested for both parameterized  $J_{1.4}$   
342 and the 3-D chemical transport model simulations. In previous studies, a number of  $\Delta G$  values have been reported: -11.02  
343 kcal mol<sup>-1</sup> (Ge et al., 2020), -15.40 kcal mol<sup>-1</sup> (Ortega et al., 2012), -13.54 kcal mol<sup>-1</sup> (Mylly et al., 2019). The  $\Delta G$  of -14.00  
344 kcal mol<sup>-1</sup> was applied in (Cai et al., 2021d) to achieve good consistencies between simulated and measured  $J_{1.4}$  is also applied  
345 in the sensitivity analysis. Figure S7 shows the variation of parameterized  $J_{1.4}$  applying different  $\Delta G$  values at 281 K, the  
346 median temperature of the observation period. For DMA with median values of ~3 ppt, different  $J_{1.4}$  could vary by ~5 orders  
347 of magnitude with  $\Delta G$  between -11.02 kcal mol<sup>-1</sup> and -15.40 kcal mol<sup>-1</sup>, while  $J_{1.4}$  with  $\Delta G$  of -13.54 kcal mol<sup>-1</sup> is also lower



348 than that of  $-15.40 \text{ kcal mol}^{-1}$  by a factor of  $\sim 10$ . However, if the DMA concentrations are up to  $\sim 30$  ppt, the differences of  $J_{1,4}$   
349 when  $\Delta G$  varies between  $-13.54 \text{ kcal mol}^{-1}$  and  $-15.40 \text{ kcal mol}^{-1}$  would become much smaller, due to the saturated formation  
350 of  $A_1B_1$  clusters. For the temperature of  $298.15 \text{ K}$ , the sensitivities of parameterized  $J_{1,4}$  are relatively larger, because the  
351 formation of  $A_1B_1$  clusters is far from saturation. Generally, the parameterized  $J_{1,4}$  could be very sensitive to different  $\Delta G$   
352 values achieved from quantum chemistry results due to the essential influence of cluster stabilities. As a result, using a lower  
353  $\Delta G$  value of  $-15.40 \text{ kcal mol}^{-1}$  in the 3-D simulations with the DMA1.4\_Mech8 scenario configuration could lead to much  
354 higher nucleation rates compared to the observation (Fig. S8). Thus we call for a more systematic performance assessment of  
355 quantum chemistry calculation methods to constrain the uncertainties of cluster thermodynamic stabilities.

356 Moreover, for the DMA source, we conduct two sensitivity scenarios of doubling (DMA2) and halving (DMA0.5) the inputted  
357 DMA emission to test the influence of limited measurements in constraining the DMA/ $\text{NH}_3$  emission ratio. As for the three  
358 sink processes, the parameters for DMA- $\bullet\text{OH}$  reaction and wet deposition reported in the literature have relatively small  
359 differences while aerosol uptake coefficient of DMA covers a wide range over two orders of magnitude. We then conduct two  
360 sensitivity scenarios using the upper ( $4.4 \times 10^{-2}$ , Upt4.4E-2) and lower ( $5.9 \times 10^{-4}$ , Upt5.9E-4) limit of aerosol uptake coefficient.  
361 All sensitivity scenarios are on the basis of the DMA1.4\_Mech8 configuration. The influence of scaled DMA emissions and  
362 varying uptake coefficients on simulated DMA concentration, PNSDs, and nucleation rate is shown in Fig. S9-S16 in the SI.  
363 As expected, the DMA concentration, especially for the nighttime spikes, is sensitive to the emission change. This causes an  
364 overestimation for DMA2 (by a factor of  $\sim 2$ ) and underestimation for DMA0.5 (by a factor of  $\sim 0.5$ ), judged by monthly  
365 averaged PNSD and nucleation rates. The sensitivity analysis for the uptake coefficient, however, shows different results. A  
366 higher uptake coefficient of  $4.4 \times 10^{-2}$  leads to a much lower DMA concentration (10% of the “best-case”) while DMA  
367 concentration only increase slightly when the lower limit of  $5.9 \times 10^{-4}$  is used. Moreover, the change in uptake coefficient show  
368 limited effect on PNSD. The reason is that the DMA concentrations during NPF periods are much less affected by the changes  
369 in uptake coefficient than those in non-NPF periods, since NPF usually occurs at low CS conditions when the uptake of DMA  
370 is weak. The sensitivity analysis above show that the parameters used in our simulation are reasonable, since perturbations  
371 within the ranges reported in the literature generally worsen the model performance. We also expect more field measurements  
372 of DMA emission and its aerosol uptake to further constrain the key source-sink process parameters in the simulation of DMA,  
373 although some of them show minor effect on NPF and PNSD simulations.

#### 374 4 Conclusions

375 This study presents a SA-DMA nucleation parameterization for application in 3-D chemical transport models. Compared to  
376 semi-empirical power-law fitting parameterizations, this new parameterization is based on the key pathway of SA-DMA  
377 cluster formation and make good representations of the coagulation scavenging effect and cluster stability. Pseudo-steady-  
378 state assumptions are applied and validated according to the short characteristic equilibrium time and through comparisons  
379 with the cluster dynamic simulations and the kinetic model. Compared with simulating the SA-DMA nucleation with cluster  
380 dynamic simulations or the kinetic model, applying this parameterization into 3-D chemical transport models would largely  
381 reduce the computational costs.

382 We incorporate this new parameterization as well as the sources and sinks of DMA into the WRF-Chem/R2D-VBS model.  
383 Using the updated model, we simulate the DMA concentrations and PNSDs in Beijing during December 2018 and January  
384 2019. Comparisons are made between 3-D model simulations and ambient measurements. Good consistency is achieved in  
385 simulating the precursor concentrations, which validates the source-sink simulation of SA and DMA. Primarily, our  
386 quantitative analysis show that compared to other nucleation mechanisms, SA-DMA nucleation would contribute to  $>99\%$  of  
387 particle formation rates and  $>60\%$  of particle number concentrations during the simulation period in urban Beijing. Although



388 the uncertainties exist due to the excess rapid growth in 3-D simulation, SA-DMA nucleation should be dominant sources of  
389 aerosol population due to its dominance in new particle formation rates. Furtherly, the 3-D simulations with this  
390 parameterization make good predictions of the CS-dependent NPF occurrence in urban Beijing and quantitatively reproduce  
391 the particle size distributions. These demonstrate that incorporating the SA-DMA nucleation parameterization including the  
392 effect of coagulation scavenging and cluster stabilities with 3-D chemical transport models would significantly improve the  
393 simulation of NPF and the particle size distributions. Such improvement would be important for further simulations of cloud  
394 condensation nuclei and the climate effects of aerosols and NPF events. The improved simulations of particle size distributions  
395 also provide more evidence for quantitatively evaluate the environmental and health effect of ultrafine particles.

396 This study has emphasized that 3-D simulations with this new parameterization could reproduce the CS-dependent particle  
397 formation rates and NPF occurrence in Beijing. As CS could vary in a relative wide range between NPF days and non-NPF  
398 days in urban atmosphere (Xiao et al., 2015; Wu et al., 2007; Deng et al., 2021), compared to semi-empirical power-law  
399 functions, this parameterization of particle formation rates would be more effective in predicting the NPF occurrence in urban  
400 atmosphere. Additionally, the particle formation rates from other nucleation mechanisms should also be suppressed by high  
401 CS, which needs further exploration and parameterizations. Our methodology of applying pseudo-steady-state assumptions to  
402 kinetic models could be important in reducing computational costs of other SA-amine nucleation systems. For instance,  
403 quantum chemistry calculations also indicate that other basic molecules like trimethylamine and diamines (Jen et al., 2016;  
404 Jen et al., 2014a), might also form relative stable clusters with SA molecules, hence the methodology of parameterizations in  
405 this study could also be extended for them.

#### 406 **Codes/Data availability**

407 The codes/data are available upon request from the corresponding author.

#### 408 **Author Contribution**

409 Y.L., J.S., B.Z., and J.J. designed the research; J.Z., M.K., and J.J. collected the observational data; Y.L., R.C., and J.J. set up  
410 and tested the parameterization; J.S., B.Z., S.W., and D.G. developed the 3-D model and performed the simulations; Y.L. and  
411 J.S. analyzed the data with the help of R.C., B.Z., and J.J.; M.S. and Y.G. presented important suggestions for the writings;  
412 Y.L., J.S., B.Z., and J.J. wrote the paper with inputs from all co-authors.

#### 413 **Competing Interests**

414 Some authors are members of the editorial board of journal *Atmospheric Chemistry and Physics*. The peer-review process was  
415 guided by an independent editor, and the authors have also no other competing interests to declare.

#### 416 **Acknowledgement**

417 Financial support from the National Natural Science Foundation of China (22188102, 92044301 and 42275110), Tencent  
418 Foundation through the XPLOER PRIZE and Samsung PM<sub>2.5</sub> SRP are acknowledged. M. Shrivastava acknowledges the  
419 support from the U.S. Department of Energy (DOE), Office of Science, Office of Biological and Environmental Research  
420 through the Early Career Research Program.



## 421 References

- 422 Almeida, J., Schobesberger, S., Kurten, A., Ortega, I. K., Kupiainen-Maatta, O., Praplan, A. P., Adamov, A., Amorim, A.,  
423 Bianchi, F., Breitenlechner, M., David, A., Dommen, J., Donahue, N. M., Downard, A., Dunne, E., Duplissy, J., Ehrhart,  
424 S., Flagan, R. C., Franchin, A., Guida, R., Hakala, J., Hansel, A., Heinritzi, M., Henschel, H., Jokinen, T., Junninen, H.,  
425 Kajos, M., Kangasluoma, J., Keskinen, H., Kupc, A., Kurten, T., Kvashin, A. N., Laaksonen, A., Lehtipalo, K., Leiminger,  
426 M., Leppa, J., Loukonen, V., Makhmutov, V., Mathot, S., McGrath, M. J., Nieminen, T., Olenius, T., Onnela, A., Petaja,  
427 T., Riccobono, F., Riipinen, I., Rissanen, M., Rondo, L., Ruuskanen, T., Santos, F. D., Sarnela, N., Schallhart, S.,  
428 Schnitzhofer, R., Seinfeld, J. H., Simon, M., Sipila, M., Stozhkov, Y., Stratmann, F., Tome, A., Trostl, J., Tsigakogeorgas,  
429 G., Vaattovaara, P., Viisanen, Y., Virtanen, A., Vrtala, A., Wagner, P. E., Weingartner, E., Wex, H., Williamson, C.,  
430 Wimmer, D., Ye, P. L., Yli-Juuti, T., Carslaw, K. S., Kulmala, M., Curtius, J., Baltensperger, U., Worsnop, D. R.,  
431 Vehkamäki, H., and Kirkby, J.: Molecular understanding of sulphuric acid-amine particle nucleation in the atmosphere,  
432 *Nature*, 502, 359-363, 2013.
- 433 Bergman, T., Laaksonen, A., Korhonen, H., Malila, J., Dunne, E. M., Mielonen, T., Lehtinen, K. E. J., Kuhn, T., Arola, A.,  
434 and Kokkola, H.: Geographical and diurnal features of amine-enhanced boundary layer nucleation, *J Geophys Res-Atmos*,  
435 120, 9606-9624, 2015.
- 436 Bertram, T. H., Kimmel, J. R., Crisp, T. A., Ryder, O. S., Yatavelli, R. L. N., Thornton, J. A., Cubison, M. J., Gonin, M., and  
437 Worsnop, D. R.: A field-deployable, chemical ionization time-of-flight mass spectrometer, *Atmos. Meas. Tech.*, 4, 1471-  
438 1479, 10.5194/amt-4-1471-2011, 2011.
- 439 Cai, R., Chen, D.-R., Hao, J., and Jiang, J.: A miniature cylindrical differential mobility analyzer for sub-3 nm particle sizing,  
440 *Journal of Aerosol Science*, 106, 111-119, <https://doi.org/10.1016/j.jaerosci.2017.01.004>, 2017a.
- 441 Cai, R., Yan, C., Worsnop, D. R., Bianchi, F., Kerminen, V.-M., Liu, Y., Wang, L., Zheng, J., Kulmala, M., and Jiang, J.: An  
442 indicator for sulfuric acid-amine nucleation in atmospheric environments, *Aerosol Science and Technology*, 55, 1059-  
443 1069, 10.1080/02786826.2021.1922598, 2021a.
- 444 Cai, R., Yan, C., Yang, D., Yin, R., Lu, Y., Deng, C., Fu, Y., Ruan, J., Li, X., Kontkanen, J., Zhang, Q., Kangasluoma, J., Ma,  
445 Y., Hao, J., Worsnop, D. R., Bianchi, F., Paasonen, P., Kerminen, V.-M., Liu, Y., Wang, L., Zheng, J., Kulmala, M., and  
446 Jiang, J.: Sulfuric acid-amine nucleation in urban Beijing, *Atmospheric Chemistry and Physics*, 21, 2457-2468,  
447 10.5194/acp-21-2457-2021, 2021b.
- 448 Cai, R. L. and Jiang, J. K.: A new balance formula to estimate new particle formation rate: reevaluating the effect of coagulation  
449 scavenging, *Atmos Chem Phys*, 17, 12659-12675, 2017.
- 450 Cai, R. L., Yang, D. S., Fu, Y. Y., Wang, X., Li, X. X., Ma, Y., Hao, J. M., Zheng, J., and Jiang, J. K.: Aerosol surface area  
451 concentration: a governing factor in new particle formation in Beijing, *Atmos Chem Phys*, 17, 12327-12340, 2017b.
- 452 Cai, R. L., Yan, C., Worsnop, D. R., Bianchi, F., Kerminen, V. M., Liu, Y. C., Wang, L., Zheng, J., Kulmala, M., and Jiang,  
453 J. K.: An indicator for sulfuric acid-amine nucleation in atmospheric environments, *Aerosol Sci Tech*, 55, 1059-1069,  
454 2021c.
- 455 Cai, R. L., Yan, C., Yang, D. S., Yin, R. J., Lu, Y. Q., Deng, C. J., Fu, Y. Y., Ruan, J. X., Li, X. X., Kontkanen, J., Zhang, Q.,  
456 Kangasluoma, J., Ma, Y., Hao, J. M., Worsnop, D. R., Bianchi, F., Paasonen, P., Kerminen, V. M., Liu, Y. C., Wang, L.,  
457 Zheng, J., Kulmala, M., and Jiang, J. K.: Sulfuric acid-amine nucleation in urban Beijing, *Atmos Chem Phys*, 21, 2457-  
458 2468, 2021d.
- 459 Cai, R. L., Yin, R. J., Yan, C., Yang, D. S., Deng, C. J., Dada, L., Kangasluoma, J., Kontkanen, J., Halonen, R., Ma, Y., Zhang,  
460 X. H., Paasonen, P., Petaja, T., Kerminen, V. M., Liu, Y. C., Bianchi, F., Zheng, J., Wang, L., Hao, J. M., Smith, J. N.,  
461 Donahue, N. M., Kulmala, M., Worsnop, D. R., and Jiang, J. K.: The missing base molecules in atmospheric acid-base  
462 nucleation, *Natl Sci Rev*, 9, 2022.
- 463 Chan, T. W. and Mozurkewich, M.: Measurement of the coagulation rate constant for sulfuric acid particles as a function of  
464 particle size using tandem differential mobility analysis, *Journal of Aerosol Science*, 32, 321-339, 2001.
- 465 Chen, D., Shen, Y., Wang, J., Gao, Y., Gao, H., and Yao, X.: Mapping gaseous dimethylamine, trimethylamine, ammonia,  
466 and their particulate counterparts in marine atmospheres of China's marginal seas – Part 1: Differentiating marine emission  
467 from continental transport, *Atmospheric Chemistry and Physics*, 21, 16413-16425, 10.5194/acp-21-16413-2021, 2021.
- 468 Chen, M., Titcombe, M., Jiang, J., Jen, C., Kuang, C., Fischer, M. L., Eisele, F. L., Siepmann, J. I., Hanson, D. R., Zhao, J.,  
469 and McMurry, P. H.: Acid-base chemical reaction model for nucleation rates in the polluted atmospheric boundary layer,  
470 *Proc Natl Acad Sci U S A*, 109, 18713-18718, 10.1073/pnas.1210285109, 2012.
- 471 Deng, C., Cai, R., Yan, C., Zheng, J., and Jiang, J.: Formation and growth of sub-3 nm particles in megacities: impact of  
472 background aerosols, *Faraday Discuss*, 226, 348-363, 10.1039/d0fd00083c, 2021.
- 473 Deng, C. J., Fu, Y. Y., Dada, L., Yan, C., Cai, R. L., Yang, D. S., Zhou, Y., Yin, R. J., Lu, Y. Q., Li, X. X., Qiao, X. H., Fan,  
474 X. L., Nie, W., Kontkanen, J., Kangasluoma, J., Chu, B. W., Ding, A. J., Kerminen, V. M., Paasonen, P., Worsnop, D. R.,  
475 Bianchi, F., Liu, Y. C., Zheng, J., Wang, L., Kulmala, M., and Jiang, J. K.: Seasonal Characteristics of New Particle  
476 Formation and Growth in Urban Beijing, *Environ Sci Technol*, 54, 8547-8557, 2020.
- 477 Dunne, E. M., Gordon, H., Kurten, A., Almeida, J., Duplissy, J., Williamson, C., Ortega, I. K., Pringle, K. J., Adamov, A.,  
478 Baltensperger, U., Barmet, P., Benduhn, F., Bianchi, F., Breitenlechner, M., Clarke, A., Curtius, J., Dommen, J., Donahue,  
479 N. M., Ehrhart, S., Flagan, R. C., Franchin, A., Guida, R., Hakala, J., Hansel, A., Heinritzi, M., Jokinen, T., Kangasluoma,  
480 J., Kirkby, J., Kulmala, M., Kupc, A., Lawler, M. J., Lehtipalo, K., Makhmutov, V., Mann, G., Mathot, S., Merikanto, J.,  
481 Miettinen, P., Nenes, A., Onnela, A., Rap, A., Reddington, C. L. S., Riccobono, F., Richards, N. A. D., Rissanen, M. P.,  
482 Rondo, L., Sarnela, N., Schobesberger, S., Sengupta, K., Simon, M., Sipilaa, M., Smith, J. N., Stozhkov, Y., Tome, A.,



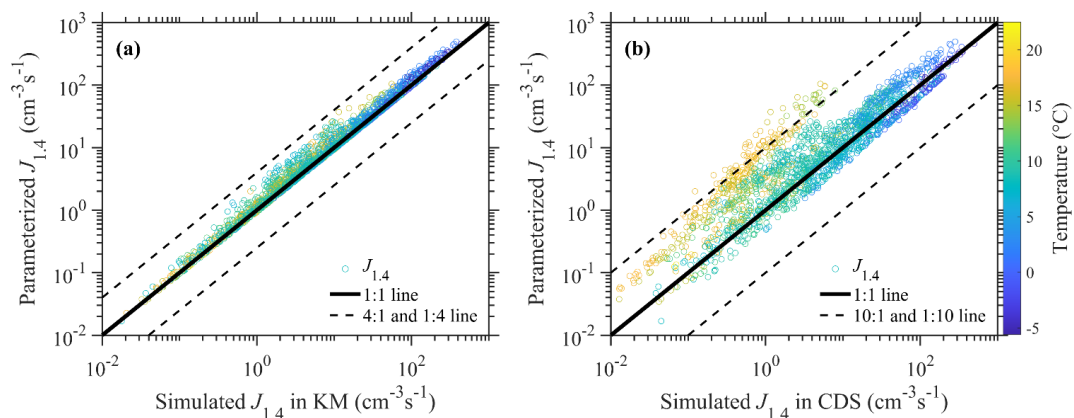
- 483 Trostl, J., Wagner, P. E., Wimmer, D., Winkler, P. M., Worsnop, D. R., and Carslaw, K. S.: Global atmospheric particle  
484 formation from CERN CLOUD measurements, *Science*, 354, 1119-1124, 2016.
- 485 Gao, M., Han, Z., Tao, Z., Li, J., Kang, J.-E., Huang, K., Dong, X., Zhuang, B., Li, S., Ge, B., Wu, Q., Lee, H.-J., Kim, C.-H.,  
486 Fu, J. S., Wang, T., Chin, M., Li, M., Woo, J.-H., Zhang, Q., Cheng, Y., Wang, Z., and Carmichael, G. R.: Air quality and  
487 climate change, Topic 3 of the Model Inter-Comparison Study for Asia Phase III (MICS-Asia III) – Part 2: aerosol radiative  
488 effects and aerosol feedbacks, *Atmospheric Chemistry and Physics*, 20, 1147-1161, 10.5194/acp-20-1147-2020, 2020.
- 489 Ge, P., Luo, G., Huang, W., Xie, H. B., Chen, J. W., and Luo, Y.: Theoretical study of the hydration effects on alkylamine and  
490 alkanolamine clusters and the atmospheric implication, *Chemosphere*, 243, 2020.
- 491 Ge, X., Wexler, A. S., and Clegg, S. L.: Atmospheric amines – Part I. A review, *Atmos Environ*, 45, 524-546,  
492 10.1016/j.atmosenv.2010.10.012, 2011.
- 493 Glasoe, W. A., Volz, K., Panta, B., Freshour, N., Bachman, R., Hanson, D. R., McMurry, P. H., and Jen, C.: Sulfuric acid  
494 nucleation: An experimental study of the effect of seven bases, *J Geophys Res-Atmos*, 120, 1933-1950, 2015.
- 495 Gordon, H., Kirkby, J., Baltensperger, U., Bianchi, F., Breitenlechner, M., Curtius, J., Dias, A., Dommen, J., Donahue, N. M.,  
496 Dunne, E. M., Duplissy, J., Ehrhart, S., Flagan, R. C., Frege, C., Fuchs, C., Hansel, A., Hoyle, C. R., Kulmala, M., Kurten,  
497 A., Lehtipalo, K., Makhmutov, V., Molteni, U., Rissanen, M. P., Stozhkov, Y., Trostl, J., Tsagkogeorgas, G., Wagner, R.,  
498 Williamson, C., Wimmer, D., Winkler, P. M., Yan, C., and Carslaw, K. S.: Causes and importance of new particle  
499 formation in the present-day and preindustrial atmospheres, *J Geophys Res-Atmos*, 122, 8739-8760, 2017.
- 500 Guenther, A., Karl, T., Harley, P., Wiedinmyer, C., Palmer, P. I., and Geron, C.: Estimates of global terrestrial isoprene  
501 emissions using MEGAN (Model of Emissions of Gases and Aerosols from Nature), *Atmos. Chem. Phys.*, 6, 3181-3210,  
502 10.5194/acp-6-3181-2006, 2006.
- 503 Hanson, D. R., Bier, I., Panta, B., Jen, C. N., and McMurry, P. H.: Computational Fluid Dynamics Studies of a Flow Reactor:  
504 Free Energies of Clusters of Sulfuric Acid with NH<sub>3</sub> or Dimethyl Amine, *J Phys Chem A*, 121, 3976-3990, 2017.
- 505 Jen, C. N., McMurry, P. H., and Hanson, D. R.: Stabilization of sulfuric acid dimers by ammonia, methylamine, dimethylamine,  
506 and trimethylamine, *Journal of Geophysical Research: Atmospheres*, 119, 7502-7514, 10.1002/2014jd021592, 2014a.
- 507 Jen, C. N., McMurry, P. H., and Hanson, D. R.: Stabilization of sulfuric acid dimers by ammonia, methylamine, dimethylamine,  
508 and trimethylamine, *J Geophys Res-Atmos*, 119, 7502-7514, 2014b.
- 509 Jen, C. N., Bachman, R., Zhao, J., McMurry, P. H., and Hanson, D. R.: Diamine-sulfuric acid reactions are a potent source of  
510 new particle formation, *Geophys Res Lett*, 43, 867-873, 10.1002/2015gl066958, 2016.
- 511 Jiang, J., Chen, M., Kuang, C., Attoui, M., and McMurry, P. H.: Electrical Mobility Spectrometer Using a Diethylene Glycol  
512 Condensation Particle Counter for Measurement of Aerosol Size Distributions Down to 1 nm, *Aerosol Science and*  
513 *Technology*, 45, 510-521, 10.1080/02786826.2010.547538, 2011.
- 514 Jokinen, T., Sipilä M., Junninen, H., Ehn, M., Lönn, G., Hakala, J., Petäjä T., Mauldin Iii, R. L., Kulmala, M., and Worsnop,  
515 D. R.: Atmospheric sulphuric acid and neutral cluster measurements using CI-API-TOF, *Atmos. Chem. Phys.*, 12, 4117-  
516 4125, 10.5194/acp-12-4117-2012, 2012.
- 517 Kulmala, M.: How particles nucleate and grow, *Science*, 302, 1000-1001, 2003.
- 518 Kulmala, M., Vehkamäki, H., Petaja, T., Dal Maso, M., Lauri, A., Kerminen, V. M., Birmili, W., and McMurry, P. H.:  
519 Formation and growth rates of ultrafine atmospheric particles: a review of observations, *J Aerosol Sci*, 35, 143-176, 2004.
- 520 Kurten, A., Li, C. X., Bianchi, F., Curtius, J., Dias, A., Donahue, N. M., Duplissy, J., Flagan, R. C., Hakala, J., Jokinen, T.,  
521 Kirkby, J., Kulmala, M., Laaksonen, A., Lehtipalo, K., Makhmutov, V., Onnela, A., Rissanen, M. P., Simon, M., Sipilä,  
522 M., Stozhkov, Y., Trostl, J., Ye, P. L., and McMurry, P. H.: New particle formation in the sulfuric acid-dimethylamine-  
523 water system: reevaluation of CLOUD chamber measurements and comparison to an aerosol nucleation and growth model,  
524 *Atmos Chem Phys*, 18, 845-863, 2018.
- 525 Kurten, A., Jokinen, T., Simon, M., Sipilä, M., Sarnela, N., Junninen, H., Adamov, A., Almeida, J., Amorim, A., Bianchi, F.,  
526 Breitenlechner, M., Dommen, J., Donahue, N. M., Duplissy, J., Ehrhart, S., Flagan, R. C., Franchin, A., Hakala, J., Hansel,  
527 A., Heinritzi, M., Hutterli, M., Kangasluoma, J., Kirkby, J., Laaksonen, A., Lehtipalo, K., Leiminger, M., Makhmutov, V.,  
528 Mathot, S., Onnela, A., Petaja, T., Praplan, A. P., Riccobono, F., Rissanen, M. P., Rondo, L., Schobesberger, S., Seinfeld,  
529 J. H., Steiner, G., Tome, A., Trostl, J., Winkler, P. M., Williamson, C., Wimmer, D., Ye, P. L., Baltensperger, U., Carslaw,  
530 K. S., Kulmala, M., Worsnop, D. R., and Curtius, J.: Neutral molecular cluster formation of sulfuric acid-dimethylamine  
531 observed in real time under atmospheric conditions, *P Natl Acad Sci USA*, 111, 15019-15024, 2014.
- 532 Lehtinen, K. E. J., Dal Maso, M., Kulmala, M., and Kerminen, V. M.: Estimating nucleation rates from apparent particle  
533 formation rates and vice versa: Revised formulation of the Kerminen-Kulmala equation, *J Aerosol Sci*, 38, 988-994, 2007.
- 534 Lehtipalo, K., Rondo, L., Kontkanen, J., Schobesberger, S., Jokinen, T., Sarnela, N., Kurten, A., Ehrhart, S., Franchin, A.,  
535 Nieminen, T., Riccobono, F., Sipilä, M., Yli-Juuti, T., Duplissy, J., Adamov, A., Ahlm, L., Almeida, J., Amorim, A.,  
536 Bianchi, F., Breitenlechner, M., Dommen, J., Downard, A. J., Dunne, E. M., Flagan, R. C., Guida, R., Hakala, J., Hansel,  
537 A., Jud, W., Kangasluoma, J., Kerminen, V. M., Keskinen, H., Kim, J., Kirkby, J., Kupc, A., Kupiainen-Maatta, O.,  
538 Laaksonen, A., Lawler, M. J., Leiminger, M., Mathot, S., Olenius, T., Ortega, I. K., Onnela, A., Petaja, T., Praplan, A.,  
539 Rissanen, M. P., Ruuskanen, T., Santos, F. D., Schallhart, S., Schnitzhofer, R., Simon, M., Smith, J. N., Trostl, J.,  
540 Tsagkogeorgas, G., Tome, A., Vaattovaara, P., Vehkamäki, H., Vrtala, A. E., Wagner, P. E., Williamson, C., Wimmer, D.,  
541 Winkler, P. M., Virtanen, A., Donahue, N. M., Carslaw, K. S., Baltensperger, U., Riipinen, I., Curtius, J., Worsnop, D. R.,  
542 and Kulmala, M.: The effect of acid-base clustering and ions on the growth of atmospheric nano-particles, *Nat Commun*,  
543 7, 2016.
- 544 Liu, J., Jiang, J., Zhang, Q., Deng, J., and Hao, J.: A spectrometer for measuring particle size distributions in the range of 3  
545 nm to 10 μm, *Frontiers of Environmental Science & Engineering*, 10, 63-72, 10.1007/s11783-014-0754-x, 2016.



- 546 Liu, Y., Yan, C., Feng, Z., Zheng, F., Fan, X., Zhang, Y., Li, C., Zhou, Y., Lin, Z., Guo, Y., Zhang, Y., Ma, L., Zhou, W., Liu,  
547 Z., Dada, L., Dällenbach, K., Kontkanen, J., Cai, R., Chan, T., Chu, B., Du, W., Yao, L., Wang, Y., Cai, J., Kangasluoma,  
548 J., Kokkonen, T., Kujansuu, J., Rusanen, A., Deng, C., Fu, Y., Yin, R., Li, X., Lu, Y., Liu, Y., Lian, C., Yang, D., Wang,  
549 W., Ge, M., Wang, Y., Worsnop, D. R., Junninen, H., He, H., Kerminen, V.-M., Zheng, J., Wang, L., Jiang, J., Petäjä T.,  
550 Bianchi, F., and Kulmala, M.: Continuous and comprehensive atmospheric observations in Beijing: a station to understand  
551 the complex urban atmospheric environment, *Big Earth Data*, 4, 295-321, 10.1080/20964471.2020.1798707, 2020.
- 552 Lu, Y. Q., Liu, L., Ning, A., Yang, G., Liu, Y. L., Kurten, T., Vehkamäki, H., Zhang, X. H., and Wang, L.: Atmospheric  
553 Sulfuric Acid-Dimethylamine Nucleation Enhanced by Trifluoroacetic Acid, *Geophys Res Lett*, 47, 2020.
- 554 Mao, J., Yu, F., Zhang, Y., An, J., Wang, L., Zheng, J., Yao, L., Luo, G., Ma, W., Yu, Q., Huang, C., Li, L., and Chen, L.:  
555 High-resolution modeling of gaseous methylamines over a polluted region in China: source-dependent emissions and  
556 implications of spatial variations, *Atmospheric Chemistry and Physics*, 18, 7933-7950, 10.5194/acp-18-7933-2018, 2018.
- 557 Marten, R., Xiao, M., Rörup, B., Wang, M., Kong, W., He, X.-C., Stolzenburg, D., Pfeifer, J., Marie, G., Wang, D. S., Scholz,  
558 W., Baccharini, A., Lee, C. P., Amorim, A., Baalbaki, R., Bell, D. M., Bertozzi, B., Caudillo, L., Chu, B., Dada, L., Duplissy,  
559 J., Finkenzeller, H., Carracedo, L. G., Granzin, M., Hansel, A., Heinritzi, M., Hofbauer, V., Kempainen, D., Kürten, A.,  
560 Lampimäki, M., Lehtipalo, K., Makhmutov, V., Manninen, H. E., Mentler, B., Petäjä T., Philippov, M., Shen, J., Simon,  
561 M., Stozhkov, Y., Tomé A., Wagner, A. C., Wang, Y., Weber, S. K., Wu, Y., Zauner-Wieczorek, M., Curtius, J., Kulmala,  
562 M., Müller, O., Volkamer, R., Winkler, P. M., Worsnop, D. R., Dommen, J., Flagan, R. C., Kirkby, J., Donahue, N. M.,  
563 Lamkaddam, H., Baltensperger, U., and El Haddad, I.: Survival of newly formed particles in haze conditions,  
564 *Environmental Science: Atmospheres*, 2, 491-499, 10.1039/D2EA00007E, 2022.
- 565 McGrath, M. J., Olenius, T., Ortega, I. K., Loukonen, V., Paasonen, P., Kurten, T., Kulmala, M., and Vehkamäki, H.:  
566 Atmospheric Cluster Dynamics Code: a flexible method for solution of the birth-death equations, *Atmos Chem Phys*, 12,  
567 2345-2355, 2012.
- 568 Merikanto, J., Spracklen, D. V., Mann, G. W., Pickering, S. J., and Carslaw, K. S.: Impact of nucleation on global CCN, *Atmos*  
569 *Chem Phys*, 9, 8601-8616, 2009.
- 570 Myllys, N., Kubecka, J., Besel, V., Alfaouri, D., Olenius, T., Smith, J. N., and Passananti, M.: Role of base strength, cluster  
571 structure and charge in sulfuric-acid-driven particle formation, *Atmos Chem Phys*, 19, 9753-9768, 2019.
- 572 Olenius, T., Kupiainen-Maatta, O., Ortega, I. K., Kurten, T., and Vehkamäki, H.: Free energy barrier in the growth of sulfuric  
573 acid-ammonia and sulfuric acid-dimethylamine clusters, *J Chem Phys*, 139, 2013.
- 574 Olenius, T., Halonen, R., Kurten, T., Henschel, H., Kupiainen-Maatta, O., Ortega, I. K., Jen, C. N., Vehkamäki, H., and Riipinen,  
575 I.: New particle formation from sulfuric acid and amines: Comparison of monomethylamine, dimethylamine, and  
576 trimethylamine, *J Geophys Res-Atmos*, 122, 7103-7118, 2017.
- 577 Ortega, I. K., Kupiainen, O., Kurten, T., Olenius, T., Wilkman, O., McGrath, M. J., Loukonen, V., and Vehkamäki, H.: From  
578 quantum chemical formation free energies to evaporation rates, *Atmos Chem Phys*, 12, 225-235, 2012.
- 579 Qiu, C., Wang, L., Lal, V., Khalizov, A. F., and Zhang, R.: Heterogeneous reactions of alkylamines with ammonium sulfate  
580 and ammonium bisulfate, *Environ Sci Technol*, 45, 4748-4755, 10.1021/es1043112, 2011.
- 581 Riccobono, F., Schobesberger, S., Scott, C. E., Dommen, J., Ortega, I. K., Rondo, L., Almeida, J., Amorim, A., Bianchi, F.,  
582 Breitenlechner, M., David, A., Downard, A., Dunne, E. M., Duplissy, J., Ehrhart, S., Flagan, R. C., Franchin, A., Hansel,  
583 A., Junninen, H., Kajos, M., Keskinen, H., Kupc, A., Kurten, A., Kvashin, A. N., Laaksonen, A., Lehtipalo, K., Makhmutov,  
584 V., Mathot, S., Nieminen, T., Onnela, A., Petaja, T., Praplan, A. P., Santos, F. D., Schallhart, S., Seinfeld, J. H., Sipilä, M.,  
585 Spracklen, D. V., Stozhkov, Y., Stratmann, F., Tome, A., Tsagkogeorgas, G., Vaattovaara, P., Viisanen, Y., Vrtala, A.,  
586 Wagner, P. E., Weingartner, E., Wex, H., Wimmer, D., Carslaw, K. S., Curtius, J., Donahue, N. M., Kirkby, J., Kulmala,  
587 M., Worsnop, D. R., and Baltensperger, U.: Oxidation Products of Biogenic Emissions Contribute to Nucleation of  
588 Atmospheric Particles, *Science*, 344, 717-721, 2014.
- 589 Sceats, M. G.: Brownian coagulation in aerosols—the role of long range forces, *J Colloid Interf Sci*, 129, 105-112,  
590 [https://doi.org/10.1016/0021-9797\(89\)90419-0](https://doi.org/10.1016/0021-9797(89)90419-0), 1989.
- 591 Seinfeld, J. H. and Pandis, S. N.: *Atmospheric Chemistry and Physics: From Air Pollution to Climate Change*, 1998.
- 592 Semeniuk, K. and Dastoor, A.: Current state of aerosol nucleation parameterizations for air-quality and climate modeling,  
593 *Atmos Environ*, 179, 77-106, 2018.
- 594 Shrivastava, M., Fast, J., Easter, R., Gustafson Jr, W. I., Zaveri, R. A., Jimenez, J. L., Saide, P., and Hodzic, A.: Modeling  
595 organic aerosols in a megacity: comparison of simple and complex representations of the volatility basis set approach,  
596 *Atmos. Chem. Phys.*, 11, 6639-6662, 10.5194/acp-11-6639-2011, 2011.
- 597 Shrivastava, M., Andreae, M. O., Artaxo, P., Barbosa, H. M. J., Berg, L. K., Brito, J., Ching, J., Easter, R. C., Fan, J., Fast, J.  
598 D., Feng, Z., Fuentes, J. D., Glasius, M., Goldstein, A. H., Alves, E. G., Gomes, H., Gu, D., Guenther, A., Jathar, S. H.,  
599 Kim, S., Liu, Y., Lou, S., Martin, S. T., McNeill, V. F., Medeiros, A., de Sá S. S., Shilling, J. E., Springston, S. R., Souza,  
600 R. A. F., Thornton, J. A., Isaacman-VanWertz, G., Yee, L. D., Ynoue, R., Zaveri, R. A., Zelenyuk, A., and Zhao, C.: Urban  
601 pollution greatly enhances formation of natural aerosols over the Amazon rainforest, *Nat Commun*, 10, 1046,  
602 10.1038/s41467-019-08909-4, 2019.
- 603 Stolzenburg, D., Simon, M., Ranjithkumar, A., Kürten, A., Lehtipalo, K., Gordon, H., Ehrhart, S., Finkenzeller, H.,  
604 Pichelstorfer, L., Nieminen, T., He, X.-C., Brilke, S., Xiao, M., Amorim, A., Baalbaki, R., Baccharini, A., Beck, L., Bräkling,  
605 S., Caudillo Murillo, L., Chen, D., Chu, B., Dada, L., Dias, A., Dommen, J., Duplissy, J., El Haddad, I., Fischer, L.,  
606 Gonzalez Carracedo, L., Heinritzi, M., Kim, C., Koenig, T. K., Kong, W., Lamkaddam, H., Lee, C. P., Leiminger, M., Li,  
607 Z., Makhmutov, V., Manninen, H. E., Marie, G., Marten, R., Müller, T., Nie, W., Partoll, E., Petäjä T., Pfeifer, J., Philippov,  
608 M., Rissanen, M. P., Rörup, B., Schobesberger, S., Schuchmann, S., Shen, J., Sipilä M., Steiner, G., Stozhkov, Y., Tauber,  
609 C., Tham, Y. J., Tomé A., Vazquez-Pufleau, M., Wagner, A. C., Wang, M., Wang, Y., Weber, S. K., Wimmer, D., Wlasits,



- 610 P. J., Wu, Y., Ye, Q., Zauner-Wieczorek, M., Baltensperger, U., Carslaw, K. S., Curtius, J., Donahue, N. M., Flagan, R.  
611 C., Hansel, A., Kulmala, M., Lelieveld, J., Volkamer, R., Kirkby, J., and Winkler, P. M.: Enhanced growth rate of  
612 atmospheric particles from sulfuric acid, *Atmos Chem Phys*, 20, 7359-7372, 10.5194/acp-20-7359-2020, 2020.
- 613 Wang, L., Lal, V., Khalizov, A. F., and Zhang, R.: Heterogeneous Chemistry of Alkylamines with Sulfuric Acid: Implications  
614 for Atmospheric Formation of Alkylammonium Sulfates, *Environmental Science & Technology*, 44, 2461-2465,  
615 10.1021/es9036868, 2010.
- 616 Wu, Z. J., Hu, M., Liu, S., Wehner, B., Bauer, S., Ssling, A. M., Wiedensohler, A., Petaja, T., Dal Maso, M., and Kulmala,  
617 M.: New particle formation in Beijing, China: Statistical analysis of a 1-year data set, *J Geophys Res-Atmos*, 112, 2007.
- 618 Xiao, S., Wang, M. Y., Yao, L., Kulmala, M., Zhou, B., Yang, X., Chen, J. M., Wang, D. F., Fu, Q. Y., Worsnop, D. R., and  
619 Wang, L.: Strong atmospheric new particle formation in winter in urban Shanghai, China, *Atmospheric Chemistry and  
620 Physics*, 15, 1769-1781, 10.5194/acp-15-1769-2015, 2015.
- 621 Yang, D., Zhu, S., Ma, Y., Zhou, L., Zheng, F., Wang, L., Jiang, J., and Zheng, J.: Emissions of Ammonia and Other Nitrogen-  
622 Containing Volatile Organic Compounds from Motor Vehicles under Low-Speed Driving Conditions, *Environmental  
623 Science & Technology*, 56, 5440-5447, 10.1021/acs.est.2c00555, 2022.
- 624 Yang, S., Liu, Z., Clusius, P. S., Liu, Y., Zou, J., Yang, Y., Zhao, S., Zhang, G., Xu, Z., Ma, Z., Yang, Y., Sun, J., Pan, Y., Ji,  
625 D., Hu, B., Yan, C., Boy, M., Kulmala, M., and Wang, Y.: Chemistry of new particle formation and growth events during  
626 wintertime in suburban area of Beijing: Insights from highly polluted atmosphere, *Atmospheric Research*, 255, 105553,  
627 <https://doi.org/10.1016/j.atmosres.2021.105553>, 2021.
- 628 Yao, L., Garmash, O., Bianchi, F., Zheng, J., Yan, C., Kontkanen, J., Junninen, H., Mazon, S. B., Ehn, M., Paasonen, P., Sipila,  
629 M., Wang, M. Y., Wang, X. K., Xiao, S., Chen, H. F., Lu, Y. Q., Zhang, B. W., Wang, D. F., Fu, Q. Y., Geng, F. H., Li,  
630 L., Wang, H. L., Qiao, L. P., Yang, X., Chen, J. M., Kerminen, V. M., Petaja, T., Worsnop, D. R., Kulmala, M., and Wang,  
631 L.: Atmospheric new particle formation from sulfuric acid and amines in a Chinese megacity, *Science*, 361, 278-281, 2018.
- 632 Yu, F.: From molecular clusters to nanoparticles: second-generation ion-mediated nucleation model, *Atmos Chem Phys*, 6,  
633 5193-5211, 2006.
- 634 Yu, F. Q. and Turco, R. P.: From molecular clusters to nanoparticles: Role of ambient ionization in tropospheric aerosol  
635 formation, *J Geophys Res-Atmos*, 106, 4797-4814, 2001.
- 636 Zaveri, R. A., Easter, R. C., Shilling, J. E., and Seinfeld, J. H.: Modeling kinetic partitioning of secondary organic aerosol and  
637 size distribution dynamics: representing effects of volatility, phase state, and particle-phase reaction, *Atmos Chem Phys*,  
638 14, 5153-5181, 2014.
- 639 Zhao, B., Shrivastava, M., Donahue, N. M., Gordon, H., Schervish, M., Shilling, J. E., Zaveri, R. A., Wang, J., Andreae, M.  
640 O., Zhao, C., Gaudet, B., Liu, Y., Fan, J., and Fast, J. D.: High concentration of ultrafine particles in the Amazon free  
641 troposphere produced by organic new particle formation, *Proc Natl Acad Sci U S A*, 117, 25344-25351,  
642 10.1073/pnas.2006716117, 2020.
- 643 Zheng, H., Cai, S., Wang, S., Zhao, B., Chang, X., and Hao, J.: Development of a unit-based industrial emission inventory in  
644 the Beijing-Tianjin-Hebei region and resulting improvement in air quality modeling, *Atmospheric Chemistry and Physics*,  
645 19, 3447-3462, 10.5194/acp-19-3447-2019, 2019.
- 646 Zheng, J., Ma, Y., Chen, M., Zhang, Q., Wang, L., Khalizov, A. F., Yao, L., Wang, Z., Wang, X., and Chen, L.: Measurement  
647 of atmospheric amines and ammonia using the high resolution time-of-flight chemical ionization mass spectrometry,  
648 *Atmos Environ*, 102, 249-259, 10.1016/j.atmosenv.2014.12.002, 2015a.
- 649 Zheng, J., Ma, Y., Chen, M. D., Zhang, Q., Wang, L., Khalizov, A. F., Yao, L., Wang, Z., Wang, X., and Chen, L. X.:  
650 Measurement of atmospheric amines and ammonia using the high resolution time-of-flight chemical ionization mass  
651 spectrometry, *Atmos Environ*, 102, 249-259, 2015b.
- 652 Zhu, S., Yan, C., Zheng, J., Chen, C., Ning, H., Yang, D., Wang, M., Ma, Y., Zhan, J., Hua, C., Yin, R., Li, Y., Liu, Y., Jiang,  
653 J., Yao, L., Wang, L., Kulmala, M., and Worsnop, D. R.: Observation and Source Apportionment of Atmospheric Alkaline  
654 Gases in Urban Beijing, *Environmental Science & Technology*, 56, 17545-17555, 10.1021/acs.est.2c03584, 2022.



655

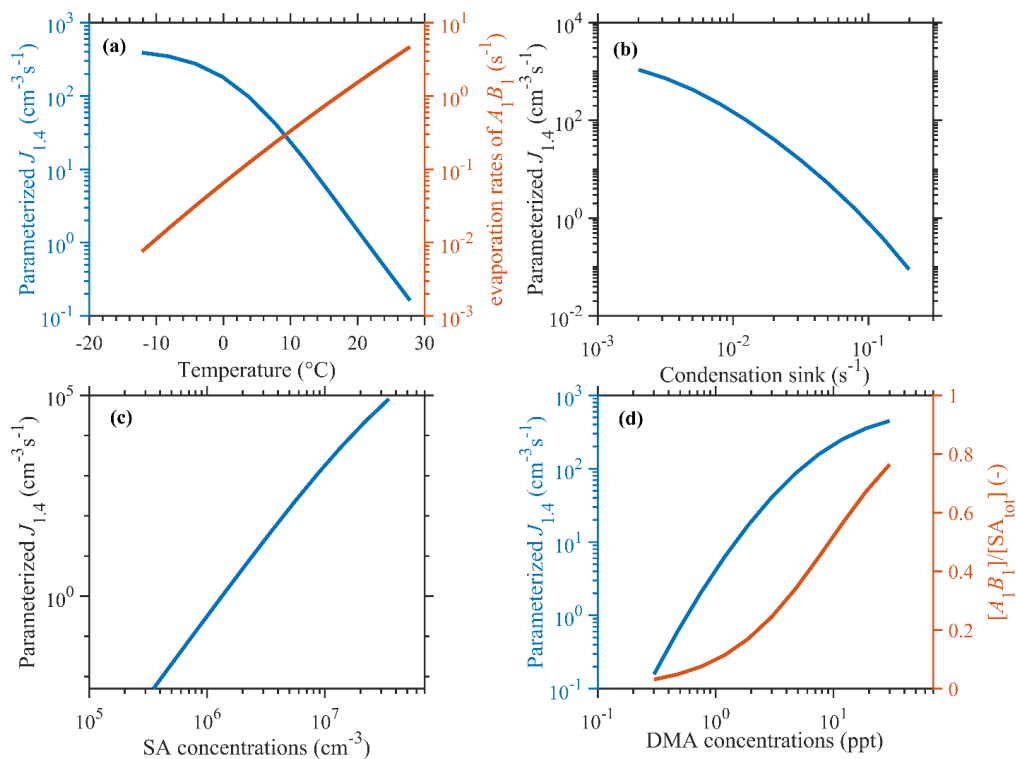
656

657

658

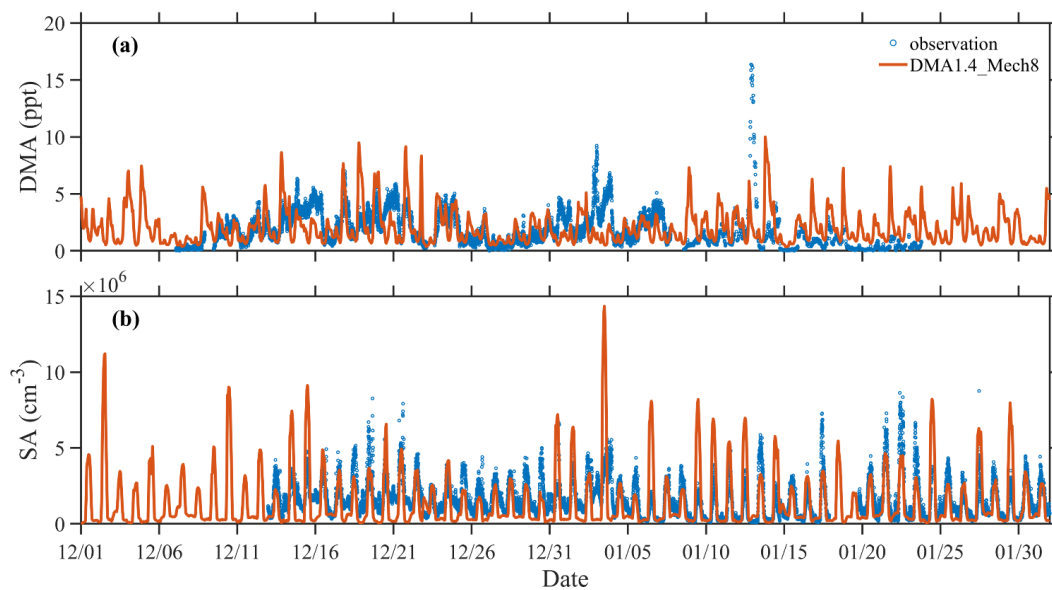
659

**Figure 1.**  $J_{1,4}$  Comparison of simplified parameterization method with kinetic model (KM) results (a) and cluster dynamic simulation (CDS) results (b). The red hollow circles showed the simulation results according to atmospheric observation data. The grey straight line represents the 1:1 line, while the grey dashed line represents the  $\pm 50\%$  variation. The circles are colored by the temperatures.



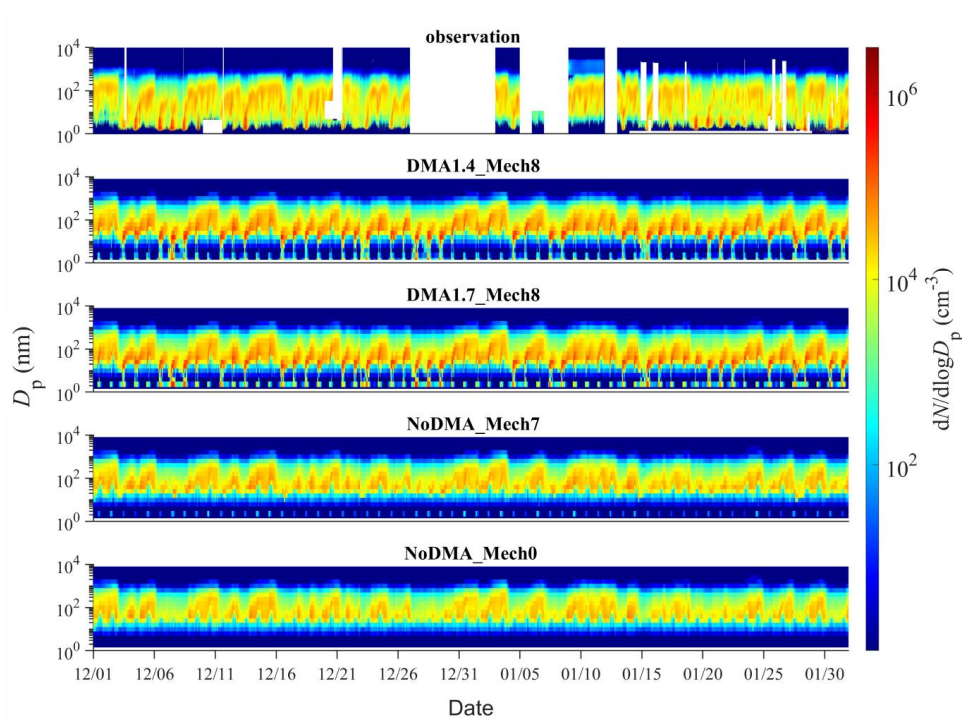
660

661 **Figure 2. Dependence of simulation results on varying  $T$ ,  $CS$ ,  $[DMA]$ ,  $[SA]$ .** The values of fixed parameters are 281K, 0.02  
662  $\text{s}^{-1}$ , 3 ppt, and  $3.5 \times 10^6 \text{ cm}^{-3}$ , respectively, as median values during NPF events in our simulation period.



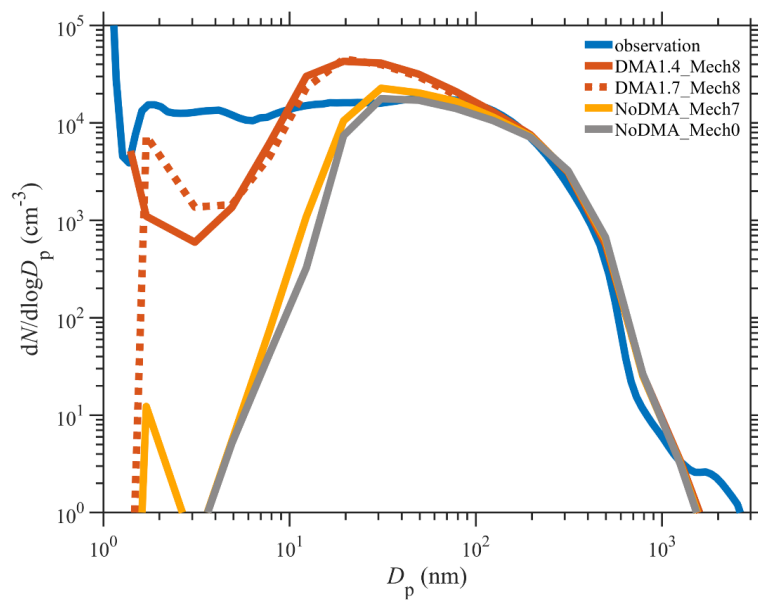
663

664 **Figure 3. Comparison of simulated concentrations of DMA (a) and SA (b) with field measurements for wintertime**  
665 **Beijing (December 2018 and January 2019).**



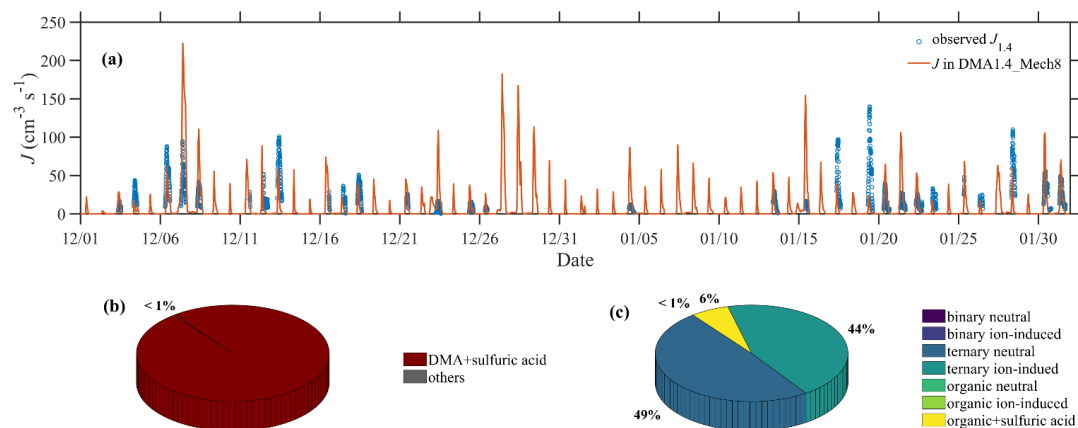
666

667 **Figure 4.** Comparison of time series of particle number size distribution simulated by various scenarios with the  
668 **observed one.** Description of four scenarios is detailed in *Configuration of the Updated WRF-Chem/R2D-VBS Model*  
669 section.



670

671 **Figure 5. Comparison of averaged particle number size distribution simulated by various scenarios with the observed**  
672 **one.** Description of four scenarios is detailed in *Configuration of the Updated WRF-Chem/R2D-VBS Model* section.



673

674 **Figure 6.** Comparison of simulated nucleation rates with those derived from field measurements (a), and contribution  
675 **from different nucleation mechanisms (b) with a special illustration of nucleation pathways other than SA-DMA (c).**